Journal of Technical Physics, J. Tech. Phys., **49**, 3–4, 267–282, 2008.
Polish Academy of Sciences, Institute of Fundamental Technological Research, Warszawa.
Military University of Technology, Warszawa.

CURRENT AND PLASMA OSCILLATION CHARACTERIZATION IN A PPS®-X000 HALL-EFFECT THRUSTER

J. KURZYNA[1], K. MAKOWSKI[2], Z. PERADZYŃSKI[3], A. LAZURENKO[4], S. MAZOUFFRE[4], G. CODUTI[4], M. DUDECK[4]

[1] **Institute of Plasma Physics and Laser Microfusion**
Hery 23, 01-497 Warsaw, Poland

[2] **Institute of Fundamental Technological Research**
Polish Academy of Sciences
Świętokrzyska 21, 00-049 Warsaw, Poland

[3] **Department of Mathematics, Computer Sciences and Mechanics**
Warsaw University
Banacha 2, 02-097 Warsaw, Poland

[4] **Laboratoire ICARE, CNRS**
45071 Orléans Cedex 2, France

The correlations between local plasma oscillations and the discharge current or cathode potential variations are studied in a high-voltage Hall-effect thruster (HET). A set of electric probes is used to collect the signals. The probes are located in the exhaust region of the thruster, beyond its outer circumference. Measurements are performed for various probe positions and bias potentials, within a wide range of thruster operating conditions. The non-stationary signals are subsequently expanded into finite sets of intrinsic modes with the use of the Empirical Mode Decomposition (EMD) method. The Hilbert–Huang power spectra indicate characteristic bands in the low frequency (LF, tens of kHz), medium frequency (MF) and high frequency (HF, tens of MHz) range. However, the regular HF emission that has been observed in our previous low-voltage characterization of a PPS-100 thruster, is only observable in some particular operating conditions. When the supply voltage is low (e.g. 400 V), the known electrostatic drift wave propagating along the thruster azimuth is unambiguously identified in the probe signals. For higher voltages, HF spectra are usually broadband and do not highlight well the defined peaks. HF emission becomes very irregular or even seemingly random. On the other hand, when regular waves appear (intermittently or in series of bursts), frequencies in the $\approx$5–100 MHz band can be observed. The oscillations within the MF band that were previously weak in the PPS-100 thruster, appear now to dominate the discharge current spectrum when the thruster operates at the highest voltages. Intense oscillations in the MF range are identified with the use of positively biased probes and by examination of the cathode potential and discharge current variations. The correlations of all the mentioned signals are clear in this frequency band. Correlating the oscillations in the HF band with the MF discharge current wave, one can deduce that HF oscillations are periodically triggered by MF waves at high voltage, while at lower voltage they are triggered by the LF breathing mode, as previously observed in the case of the PPS-100 thruster.

1. Introduction

The PPS®-X000 HET being currently under investigations at *ICARE–CNRS* is a high-voltage successor of the PPS-100. It achieves a maximal thrust of the order of 330 mN and a specific impulse of the order of 3200 s under a discharge voltage of 1 kV, with a discharge power of $\sim$ 6 kW (Ref. [1]). With a thrust four times greater than that of a PPS-100 under a xenon flow rate lower than twice that of its predecessor, this thruster is a promising device for propulsion of the future space missions.

The characterization of discharge and plasma instabilities is essential in assessment of the operational envelope of the thruster. To this end, both the discharge current and local plasma oscillations have been studied in the present experiment. The discharge current was measured directly in the electrical circuit of the thruster. In addition, the time variations of the thruster cathode potential relative to the ground were measured. The related local plasma oscillations were measured with a set of electric probes operating either close to the ground potential or with a positive or negative voltage bias. The plasma oscillations were recorded for a discharge voltage in the range 200–900 V, while the xenon mass flow rate was varied from 5 to 9 mg/s. In these series of measurements, the magnetic field was kept constant.

A cursory visual inspection of the signals collected suffices to recognize their non-stationarity and intermittent nature over the duration of the measurements. For this reason, these signals were analyzed by means of the *Empirical Mode Decomposition* method recently devised by N. HUANG (Ref. [2]). The workings of this method are summarized in the next section. In the subsequent section, a brief description of the experiment is presented. Finally, the obtained results are discussed.

2. Empirical Mode Decomposition

The well-known Fourier methods are generally not appropriate for non-stationary signals, because the "frequency content" of any interval of the non-periodic signal varies in time. For this reason, the *instantaneous frequency* and its corresponding power are often considered more relevant than Fourrier power spectra, for instance when frequency-modulated signals are considered. The instantaneous frequency is usually defined as the time derivative of the phase of a complex function $z(t)$ that is to be built using a given real signal $s(t)$ and a function $\widetilde{s}(t)$ orthogonal to the real signal (see e.g. Ref. [3]).

The intensity and rate of variation of the analyzed signal can then be determined at any moment in time. However, the orthogonal function $\widetilde{s}(t)$ is not uniquely defined. According to the definition of the complex function $z(t)$ given by GABOR [4], its Fourier transform must be identical to that of the real signal $s(t)$ for positive frequencies and must vanish for negative frequencies. It is easy to show [4, 5] that when the imaginary part of the complex function $z(t)$ is defined as the Hilbert transform of its real part, both conditions are simultaneously fulfilled. Therefore, we shall define the complex signal as $z(t) = \mathcal{A}[s(t)] \stackrel{\text{def}}{=} s(t) + i\mathcal{H}[s](t)$ where:

$$\mathcal{H}[s](t) \stackrel{\text{def}}{=} \frac{1}{\pi} \operatorname{Pv} \int_{-\infty}^{\infty} \frac{s(\tau)}{t-\tau} d\tau \stackrel{\text{den}}{=} \widetilde{s}(t)\,, \tag{2.1}$$

is the Hilbert transform of $s(t)$, and Pv the principal value of the integral. $\mathcal{A}[s(t)]$ is called an *analytical signal.* Writing $z(t)$ in the form $A(t)\exp(i\varphi(t))$, the instantaneous frequency of the analytical signal is defined as the derivative of the complex phase, $\omega_I(t) \stackrel{\text{def}}{=} d\varphi(t)/dt$ and the instantaneous power as the square of its amplitude $A(t)$, where as usual $A(t) \stackrel{\text{def}}{=} \sqrt{s^2(t) + \widetilde{s^2}(t)}$.

However, for a wide class of signals, the instantaneous frequency can become negative and may lose its physical meaning. Such signals are often called multi-component. A solution to this problem consists in representing a given multi-component signal as a sum of k simpler components $s_k(t)$ (*mono-component signals*) with well-behaved instantaneous frequency $\omega_k(t)$. Thus, one can write:

$$s(t) = \sum_{k=1}^{N} s_k(t) = \Re\left[\sum_{k=1}^{N} a_k(t)\exp(i\varphi_k(t))\right] = \Re[A(t)\exp(i\varphi(t))]\,, \tag{2.2}$$

where each elementary analytical signal $\mathcal{A}_k[s_k(t)] = s_k(t) + i\mathcal{H}[s_k](t) = z_k(t)$ is determined by $s_k(t)$ and its Hilbert transform. For each term of the sum one can find its amplitude, $a_k(t)$, and instantaneous frequency, $\omega_k(t) = \dot{\varphi}_k(t)$.

In the complex plane, mono-component signals are represented by trajectories $z_k(t)$ rotating around a fixed center. Such trajectories are called *proper rotations* [6]. By contrast, the complex trajectory of a multi-component signal describes a number of loops around moving, instantaneous centers of rotation. The complex arguments of such trajectories are consequently non-monotonic functions of time and the instantaneous frequency has no clear physical meaning.

After expansion of the multi-component signal into a set of mono-component terms, the power carried by each term is a function of time and of the instantaneous frequency. Hence, the resulting power spectrum of a non-stationary signal may be composed of several components (modes) that depend on two variables: time and instantaneous frequency. The Empirical Mode Decomposition (EMD) method provides a self-adaptive algorithm able to expand a wide class of signals into a sum of simpler, monocomponent signals – *intrinsic mode functions – imf's* [2]. Quite often, intrinsic modes have a clear interpretation and represent physical modes that arise in the process being investigated. That is what makes the EMD method particularly attractive, despite the low maturity of its underlying mathematical foundation. A power spectrum built up of instantaneous frequencies calculated for a set of intrinsic mode functions is called a *Hilbert–Huang spectrum.* Summarizing,

- a given non-stationary signal can be self-adaptively decomposed into a set of monocomponent intrinsic modes with the use of the EMD method;
- the application of the Hilbert transform to the whole set of modes allows to identify peculiar events and assign them a range of instantaneous frequency and power.

For a detailed description of the method, the Reader is referred to HUANG'S *et al.* original paper (Ref. [2]) and to the review paper (Ref. [7]). Only a succinct summary of the method shall be provided here. Let us start with the definition of the intrinsic mode functions generated by the EMD method.

DEFINITION 1: *An* ***intrinsic mode function*** $imf(t)$ *must fulfill two conditions:*

1. *The number of its zero crossings points and extrema may differ at most by one;*

2. *$imf(t)$ needs to be symmetric with respect to its local mean value which must tend to zero at any point.*

The determination of a *local mean value* $m(t)$ for a given $s(t)$ is crucial for the EMD method. Usually, this is done by calculating the average value of the *upper* $\mathrm{upp}(t)$ and *lower* $\mathrm{low}(t)$ *envelopes* of $s(t)$. The appropriate envelopes are usually interpolated using natural cubic splines joining the maxima (for $\mathrm{upp}(t)$) or minima (for $\mathrm{low}(t)$) of $s(t)$. Other possibilities exists, however: one can for instance approximate $m(t)$ with a B-spline with knots taken in all local maxima and minima of $s(t)$ [8], thus alleviating the need to explicitely determine the envelopes. The authors have tested this approach and found it equally useful as the original method of HUANG (Ref. [2]). The EMD algorithm can be summarized as follows:

- The difference between the signal $s(t)$ and the local mean $m(t)$ constitutes the first *intrinsic mode function* candidate.
- If the conditions of Definition 1 are not satisfied, the local mean of the first candidate is determined and subtracted from the first candidate, hence providing a second candidate. This procedure is applied recursively until the function can be deemed an intrinsic mode (this iterative process is called the *sifting procedure*).
- The obtained intrinsic mode is now subtracted from the raw signal to obtain a residue, or from the previous residue if such has been priorly calculated.
- The residue is processed in the same manner and the procedure is applied recursively to obtain the second and the following intrinsic modes, until the last residue contains less than two extrema.
- Finally, the Hilbert transform is applied to the whole set of intrinsic modes resulting in a *time–instantaneous frequency–power* distribution and in the desired Hilbert–Huang spectrum.

The EMD method has been successfully applied to study the HET plasma oscillations measured by an array of antennas and electric probes galvanically coupled to the plasma [9–13]. In those papers, one can find more details about the calculation of analytical signals and instantaneous frequencies, the construction of Hilbert–Huang and marginal power spectra, the determination of phase locks and the identification of possible error sources. The current study is essentially a continuation of our previous work aimed at characterizing the high voltage operation of the PPS®-X000 thruster.

3. Experiment

The PPS®-X000 HET has been operated in the PIVOINE ground-test facility [14] located at ICARE-CNRS. The new thruster is designed for discharge voltages up to twice that of its predecessor, the PPS-100. A number of measurements have been performed to study the operation of the new thruster (stability of the discharge current, efficiency *etc.*) under different conditions. The discharge voltage was varied in the range 200–900 V and the xenon flow rate in the range 5–9 mg/s. We are mainly concerned with the correlation between local oscillations (or instabilities) of the plasma in the thruster exhaust region and the global oscillations of the discharge current and cathode potential.

Discharge current oscillations were directly monitored in the thruster power circuit by means of a Tektronix current probe connected to a Tektronix TDS5104 oscilloscope. The discharge current I_A was measured at the anode of the thruster. In some experiments, the total current was measured at the cathode (I_C). The cathode potential, when recorded, was measured relative to the ground level.

Local MF and HF oscillations were recorded with the use of electric probes located on the outer circumference of the thruster, close to the plane where the magnetic field reaches its maximum [15]. Classical Langmuir probes in galvanic contact with the plasma were used. The signals were recorded with the oscilloscope operating in AC mode, at a sampling frequency of 1.25 GHz. All transmission lines were of equal length and terminated with a matching 50 Ω impedance. In some experimental sessions, the bias of the probes was varied in the range of −30–+50 V (in 10 V steps). In most cases, however, the probes were not actively biased and were effectively operating with a potential close to that of the ground.

The location of the probes is shown in Figs. 1a and 1b. Four millimeter-long probe tips with diameter 0.2 mm were oriented radially. The P_1 and P_2 probes constitute a stiff tandem with a tip separation of 10 mm or 11 mm. When the tandem was oriented in the (r, z) plane, the signal of probe P_3 was also recorded. The angle between the P_3 probe and the (r, z) plane of the tandem was constant and equal to $\pi/2$ – see Fig. 1b.

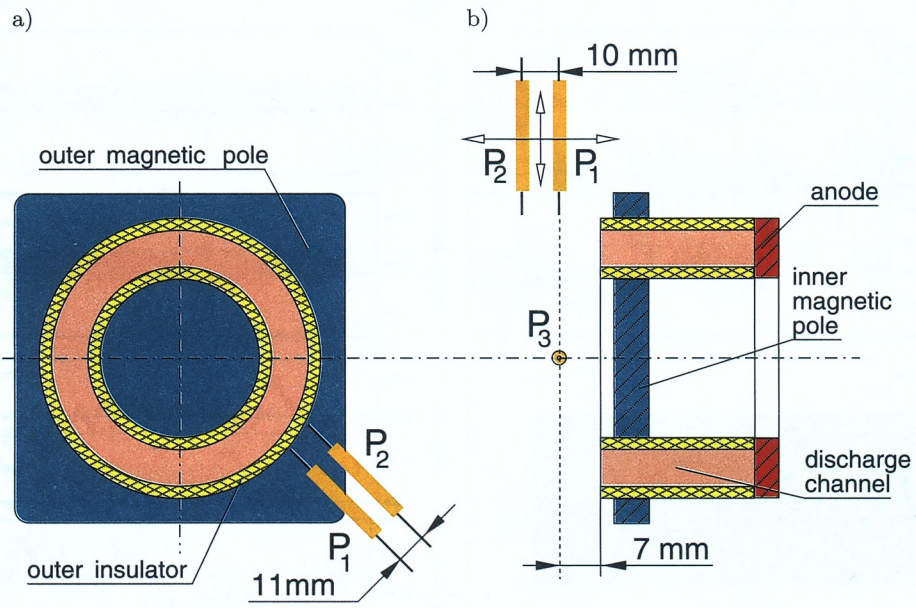

FIG. 1. Electric probes used in the experiment: a) P_1 and P_2 probe tandem at a given location in the (r, ϑ) plane, b) P_1 and P_2 probe tandem at a given azimuthal location in the (r, z) plane. The azimuthal angle between the P_3 probe and the P_1–P_2 plane is $\pi/2$.

The propagation of HF waves along the discharge channel circumference was studied with two probes located at different azimuthal positions in the same (r, ϑ) plane. When the tandem was located in the (r, z) plane of the thruster, the 10 mm separation between probe tips allowed us to follow the longitudinal propagation. In a number of

experimental sessions, the r and z coordinates of the P_1-P_2 tandem were varied. However, the probes were always kept in the shade of the outer insulator to prevent them from being directly exposed to the plasma beam.

4. Results and Discussion

The non-stationary signals corresponding to the discharge current, cathode potential and electric probe currents were studied on the basis of the raw signals and of their expansion into intrinsic mode functions using the EMD. The signals were collected for different operating conditions: the discharge voltage was varied in the range 200–900 V and the xenon flow rate in the range 5–9 mg/s.

4.1. Lower voltage range: $U_D \leq 550$ V

4.1.1. P_1 and P_2 probes in the (r, ϑ) plane, 6 mg/s xenon flow rate. A comparison between the waveforms of U_C and the discharge current shows that the period between successive cathode potential extrema is twice shorter than the breathing mode period exhibited by I_C or I_A. Typical waveforms of the corresponding raw signals are presented in Figs. 2a and 2b for discharge voltages $U_D = 350$ V and $U_D = 550$ V, respectively.

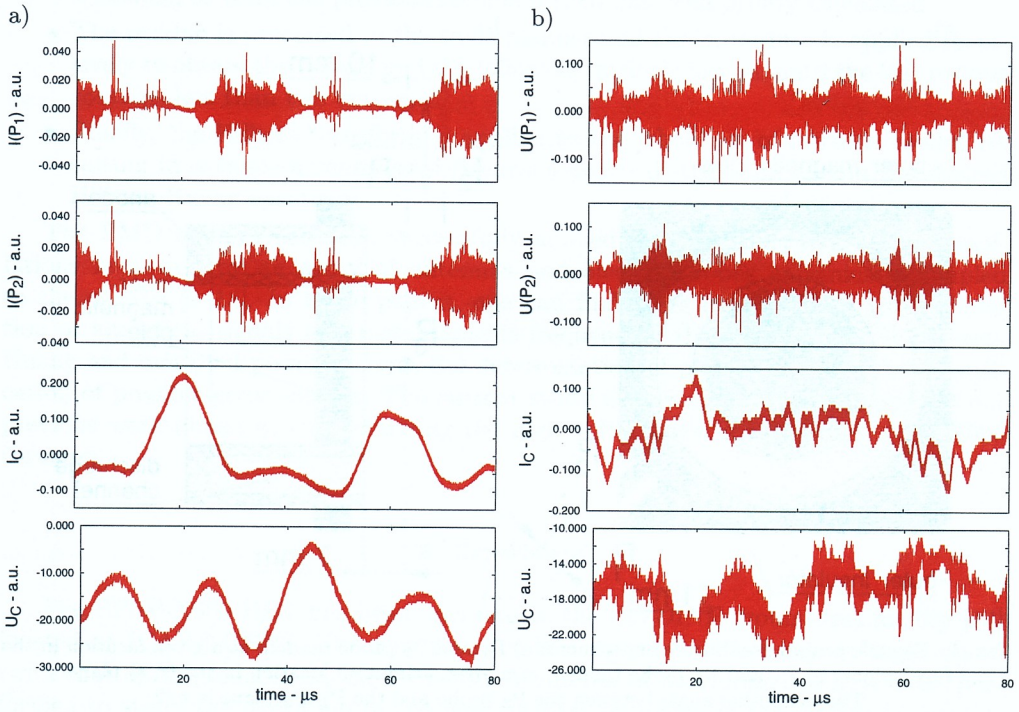

FIG. 2. Raw signals $I(P_1)$, $I(P_2)$, I_C and U_C recorded for a xenon flow rate of 6 mg/s with the P_1 and P_2 probes located in the (r, ϑ) plane; a) $U_D = 350$ V, b) $U_D = 550$ V.

A visual inspection of the waveform of I_C for $U_D = 550$ V shows significant MF oscillations superimposed on the breathing mode. They are also easily identified in the

raw U_C signal despite a significantly greater noise level than in the I_C signal. The corresponding intrinsic modes are extracted with the EMD method. The instantaneous frequency band of these MF oscillations (~ 200 kHz and higher) corresponds to the characteristic frequency of transit-time oscillations [16, 17] that might be expected for this thruster.

The P_1 and P_2 probes were not actively biased in this series of measurements. Therefore, both probes were operating close to the ground potential (possibly in the vicinity of the low knee of the $I-V$ probe characteristics to be discussed later). The MF wave could not be reliably resolved despite the high sensitivity of the conventional EMD method, whereas the HF emission was perfectly resolved.

The repeatability of the I_C and U_C signals collected in several experimental sessions is satisfactory for $U_D = 350$ V.

4.1.2. P_1 and P_2 probes in the (r, ϑ) plane, xenon flow rate 7.3 mg/s, $U_D = 350$ V. In this series of measurements, the discharge current measured on the anode side and the cathode potential are used as global reference signals. The P_2 probe was not actively

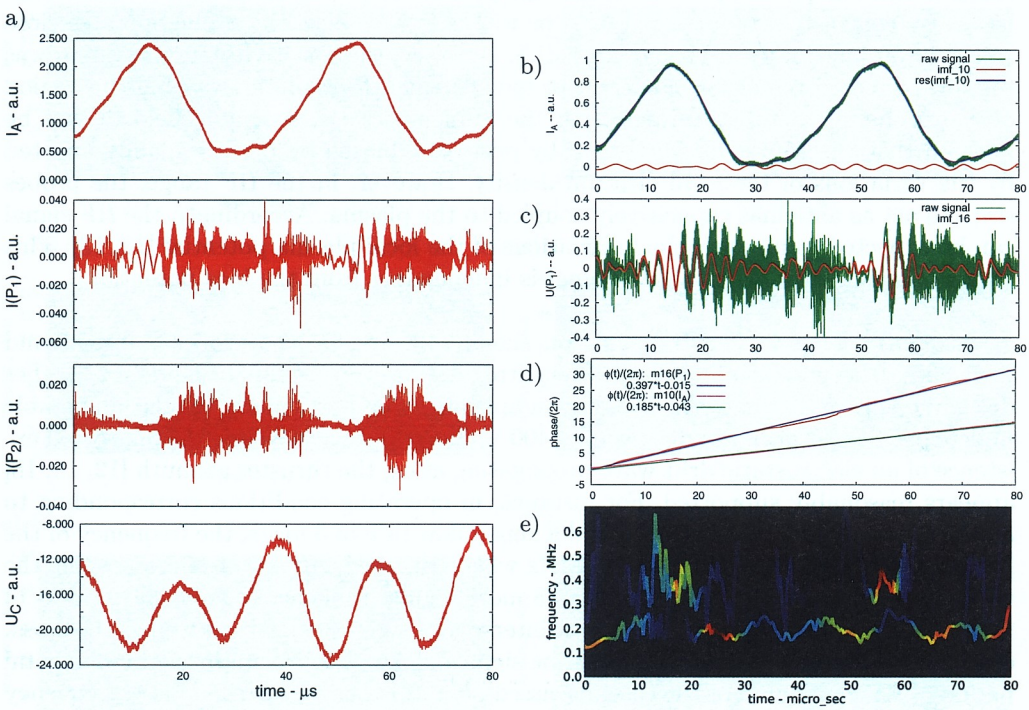

FIG. 3. P_1 and P_2 probes in the (r, ϑ) plane, xenon flow rate 7.3 mg/s, $U_D = 350$ V: a) Discharge current I_A, probe currents $I(P_1)$, $I(P_2)$ and potential U_C relative to the ground – raw signals, b) Normalized discharge current I_A (in green), its intrinsic mode imf_{10} (in red) and the residue $res(imf_{10})$ (in blue), corresponding to the *breathing mode*, c) Normalized $I(P_1)$ signal (in green) and intrinsic mode imf_{16} (in red) corresponding to a $\approx$0.4 MHz mode – probe biased at +40 V, d) Phase $\varphi(t)$ calculated for intrinsic mode $imf_{10}(I_A)$ of the discharge current I_A and $imf_{16}(P_1)$ of the P_1 probe signal. The slopes of the linear fits correspond respectively to $\approx$0.2 and $\approx$0.4 MHz, e) Hilbert spectra of the appropriate intrinsic modes for the P_1 probe (upper curve) and discharge current I_A (lower curve) – MF range.

biased, in contrast to the previous case. However, the voltage applied to the P_1 probe was varied in the range 0–50 V in steps of 10 V. Also, some measurements have been performed with P_1 biased at -20 V. Sample raw signals corresponding to I_A, U_C, to the currents of the positively biased P_1 probe and the non-biased P_2 probe are reproduced in Fig. 3a. The dominating modes extracted with the EMD method and the corresponding Hilbert–Huang spectrum in the MF range are shown on the right panels of the same figure.

The average frequency of the fastest intrinsic mode of the I_A signal amounts to $\approx$ 200 kHz. The average frequency of the corresponding intrinsic mode extracted from the positively biased probe signal is about twice larger. No such mode could be extracted with the EMD method for signals collected with probes without active bias or with negative voltage bias.

The $I - V$ probe characteristics for a PPS®-X000 thruster operating under similar conditions have been analyzed in Ref. [15]. These latter results and the maximal amplitudes of the MF oscillations recorded in the present work under different probe bias voltages suggest that even at +50 V, the electron saturation current has not been reached and the probe operates within the positive slope region of its I–V characteristics. By contrast, without active bias or with a -20 V bias, the probe operates close to the lower knee of its I–V characteristics. However, the sensitivity of our system was too low to record the electron current or ion current MF oscillations within this region of the probe characteristic. Neglecting the influence of the magnetic field, it can be inferred that the MF signals collected by positively biased probes are mainly affected by the variations of the local electron density. However, in the HF range, the probes seem to act as antennas capacitively coupled to the plasma. Accordingly, the HF signal can be expected to measure the fluctuations of the local plasma potential [12, 13]. This may explains in turn why the HF signal is independent from the bias potential.

4.1.3. HF emission. The HF emission signal collected by the probes is broadband ($\sim$ 5–200 MHz) and usually becomes very irregular or even seemingly random at higher discharge voltages. However, HF emission appears to be particularly regular and stable under specific operating conditions (e.g. 400 V, 5 mg/s). In such cases, the purported existence of an electrostatic drift wave propagating along the thruster azimuth [12, 15, 18] appears reasonably supported. For instance, in operating conditions corresponding to a discharge voltage of $U_D = 400$ V and a xenon flow rate of 5 mg/s, the frequency of the HF emission is initially about 40–50 MHz when triggered. After 2–4 microseconds, the waveform of the HF emission turns into a more regular sequence of very sharp peaks of variable amplitude. The nearly constant intervals between the peaks as well as the cross-correlations between the P_1 and P_3 probe signals allow us to calculate the fundamental period of HF emission. For the case discussed here, this period corresponds to frequency from $\approx$6.4 MHz to $\approx$6.7 MHz depending on the discharge current peak considered. The time delay Δt measured between the signals of the P_1 and P_3 probes is equal to $\approx$41 ns, which corresponds to an angular frequency $\omega = 2\pi\nu \approx 2\pi \cdot 6.1 \times 10^6$ rad/s. This translates into an azimuthal propagation velocity at the outer diameter of the channel (0.15 m) equal to $v_\vartheta \approx 2.9 \times 10^6$ m/s. Assuming that this value corresponds to the electron drift velocity along the azimuth in a radial magnetic field $B_r = 15$ mT, the axial electric field can be estimated as $E_z = v_\varphi B_r \approx 4.3 \times 10^4$ V/m. This value is about 50% greater than that reported for the PPS-100 thruster. A close estimate of the

electric field, $E_z = v_\vartheta B_r \approx 4.45 \times 10^4$ V/m, can be obtained from the signal of probe P_4. When used, the P_4 probe was located on the same diameter but opposite to the P_1 probe.

In most cases, at low voltages (e.g. $U_D = 350$ V and xenon flow rate of 5, 6 or 7.3 mg/s) the HF emission bursts are correlated with the decreasing phase of the *breathing mode* component of the discharge current. The same behavior has been previously observed in the case of PPS-100 HET. By contrast, for $U_D = 550$ V, additional MF oscillations are observed in global signals and HF emission is nearly uninterrupted. It is worth noting that the HF intensity is irregular and prone to abrupt variations. For both U_D voltages considered, the peaks at 7, 14, 19, 27, 60 and 110 MHz are clearly distinguishable in the HF power spectra.

A study of the Hilbert–Huang power spectra of the probe signals at $U_D = 350$ V reveals similar average frequencies as those observed above. However, these correspond to particular intrinsic modes and represent events that appear only sporadically in time – see Fig. 4.

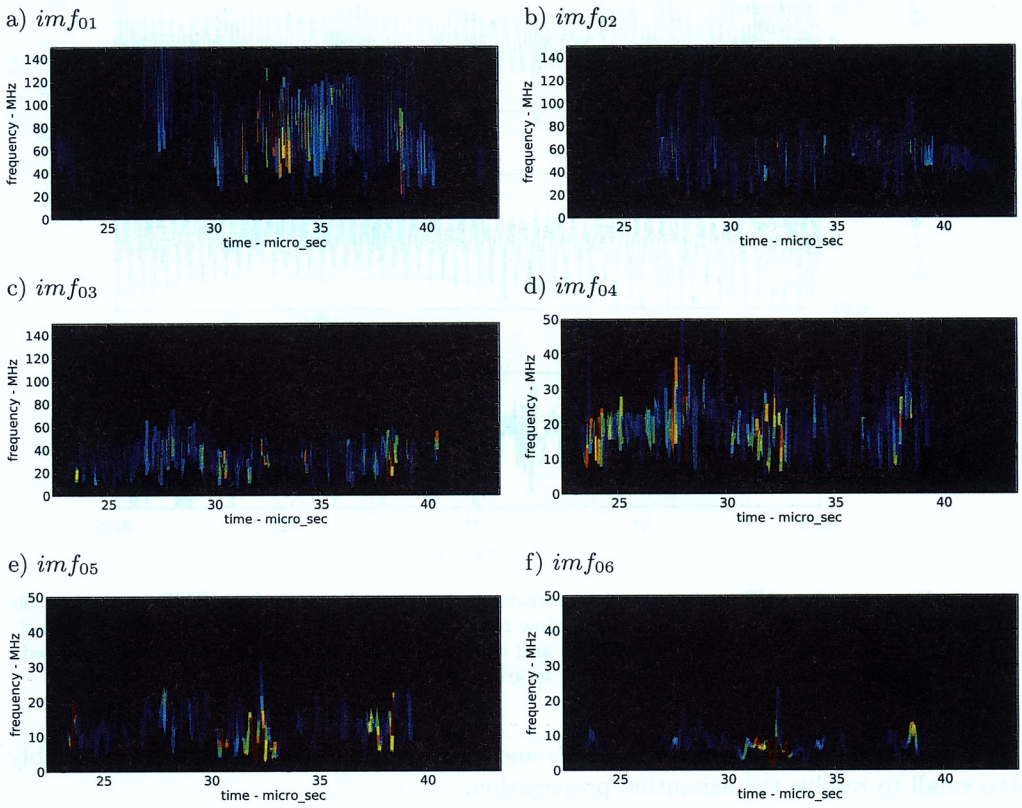

FIG. 4. Hilbert power spectra of HF intrinsic modes numbered 01–06, obtained by application of the EMD to the P_1 probe signal for $U_D = 350$ V and xenon flow rate 7.3 mg/s – the probe was not actively biased.

Upon triggering in the decreasing phase of the breathing mode, HF emission initially exhibits regular oscillations of the order of 60 MHz (see Fig. 5a). This phase may last for

about 1 μs, and may be followed by the appearence of yet faster oscillations, grouped into a sequence of wave packets. The frequency within each wave packet is modulated and reaches 100 MHz or more (Fig. 5b). The duration of the visible wave packets corresponds to the expected azimuthal electrostatic wave period. Additionally, some events characterized by more regular oscillations with frequency of about 20 MHz are observed (Fig. 5c). The slowest intrinsic modes within the HF band (here imf_{06}) follow the modulation of the wave packets envelope (Fig. 5d).

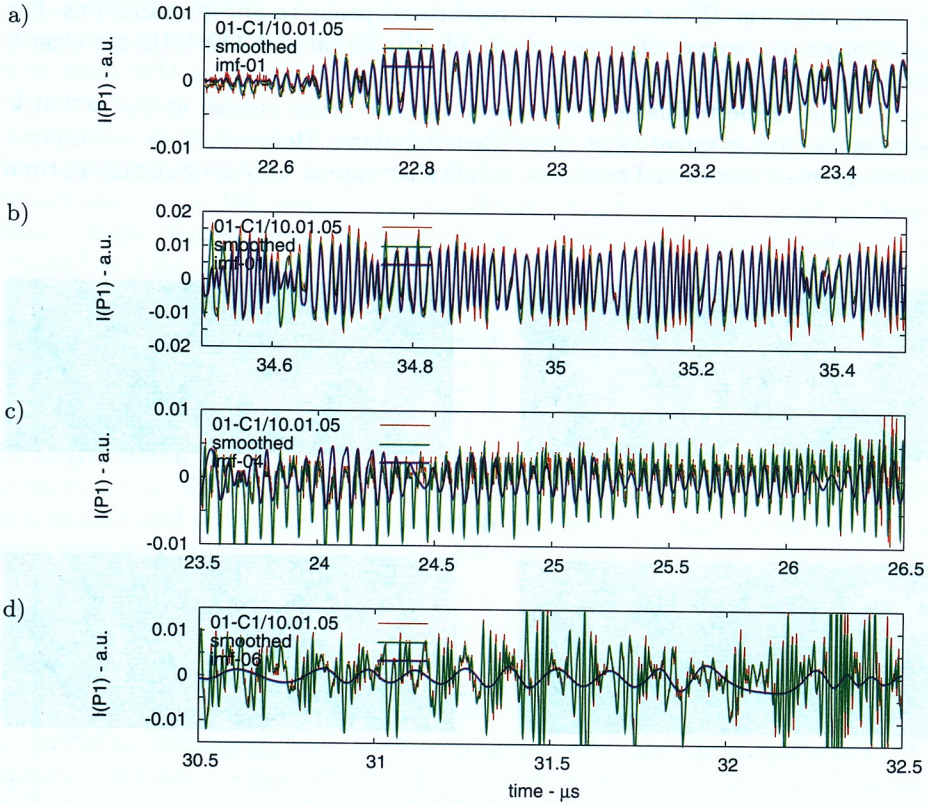

FIG. 5. Expansion into HF intrinsic modes resulting from the application of the EMD method to the P_1 probe signal with $U_D = 350$ V and xenon flow rate 7.3 mg/s – the probe was not actively biased; a) and b) imf_{01} samples, c) – imf_{04} samples and d) – imf_{06} sample. Raw signals are shown in red, signals smoothed with Gaussian filter in green, and intrinsic mode functions in blue.

The 11 mm separation between the P_1 and P_2 probes in the (r, ϑ) plane is presumably too small to resolve the azimuthal propagation.

4.2. Upper voltage range: $U_D > 500$ V. The results discussed in this section were obtained for a reduced xenon flow rate of 5 mg/s. The P_1 and P_2 probes were located in the (r, z) plane – see Fig. 1b. All three probes P_1, P_2, and P_3 were left without active bias. Typical raw signals are reproduced in Fig. 6 for various discharge voltages, $U_d = 500$, 700, and 900 V. It can be readily noticed that the waveform of the discharge

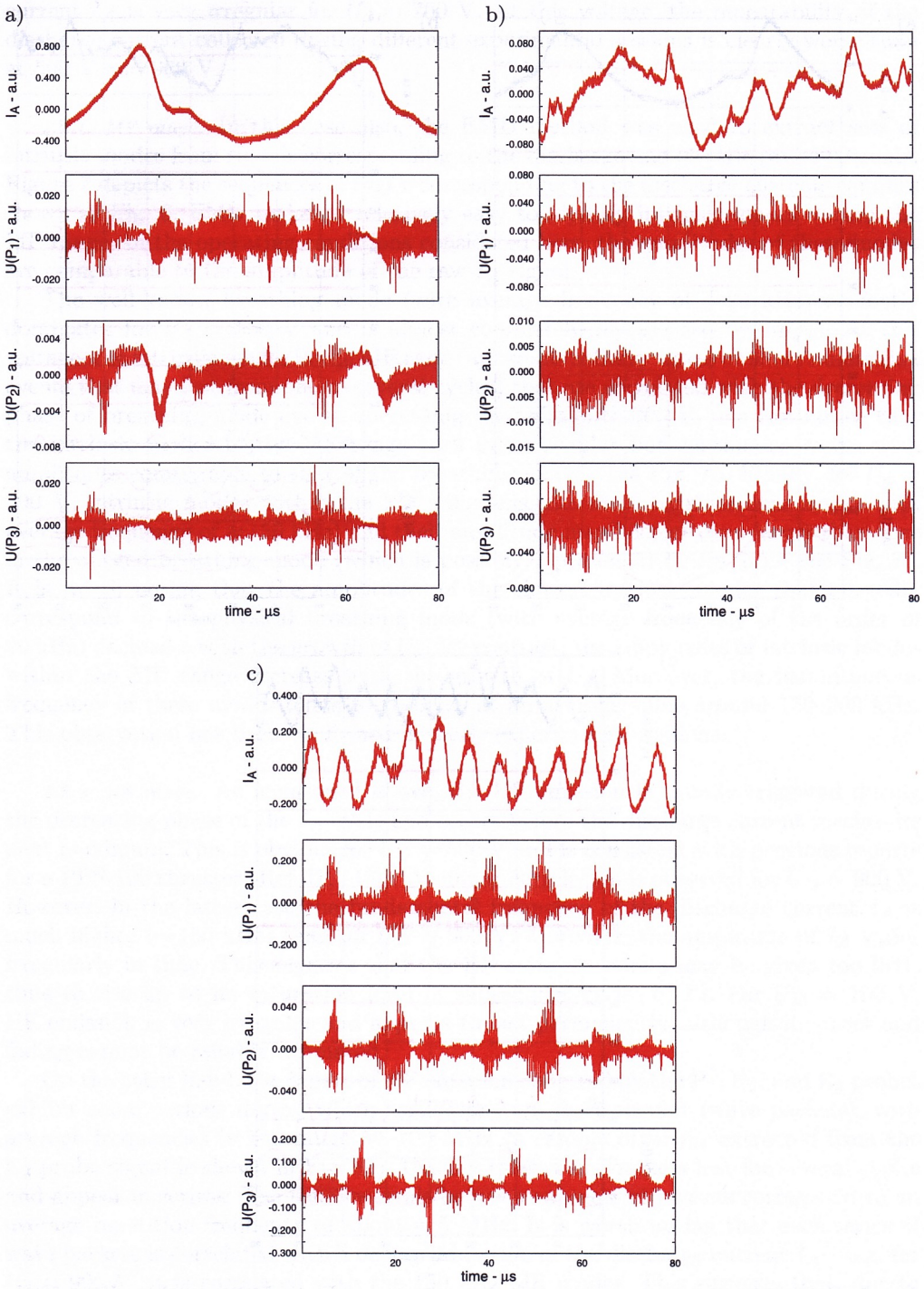

FIG. 6. Raw signals corresponding to discharge current I_A and to the currents of the P_1,P_2, and P_3 probes – 5 mg/s xenon flow rate; a) $U_D = 500$ V, b) $U_D = 700$ V, c) $U_D = 900$ V.

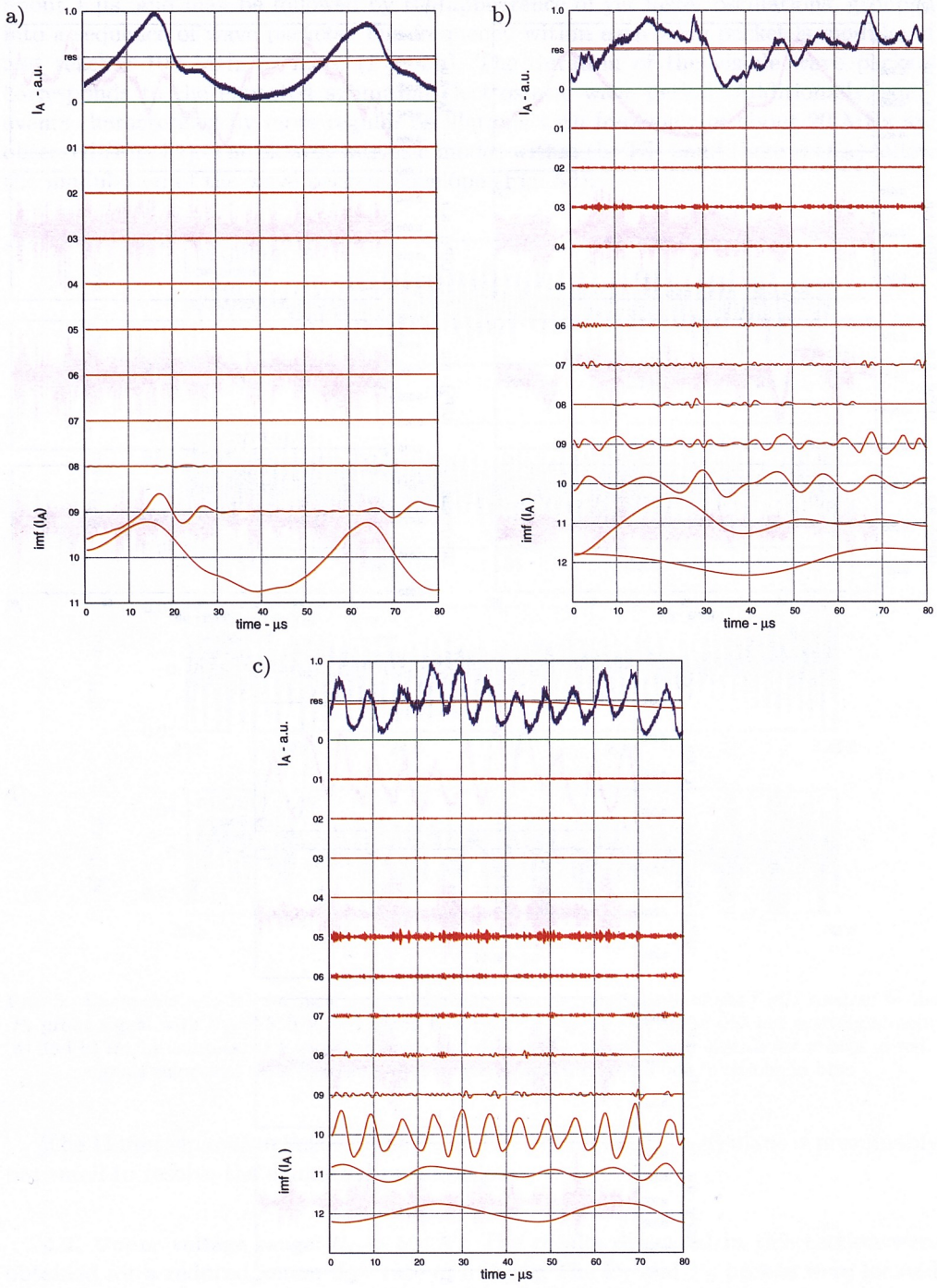

FIG. 7. Empirical mode decomposition of the discharge current I_A: a) discharge voltage $U_D = 500$ V, b) $U_D = 700$ V, and c) $U_D = 900$ V. Raw signals are shown in blue and the resulting intrinsic modes in red. Xenon flow rate of 5 mg/s.

current I_A is very irregular for $U_d = 700$ V. At this voltage, the repeatability of the discharge current collected during different experimental sessions is clearly worse than at 500 V and 900 V.

4.2.1. MF range. In this case also, the EMD method was used to extract sets of intrinsic modes from signals corresponding to the discharge and electric probe currents. Figure 7 depicts the sequences of imf's corresponding to the discharge currents samples shown in Fig. 6. EMD makes it relatively easy to identify intrinsic modes within the MF range. In the operating conditions considered here, the amplitudes of these modes are comparable to the amplitude of the raw I_A signal.

The well-known breathing mode (with average frequency of ~ 20 kHz) evidently dominates for $U_d = 500$ V and is almost completely represented by imf_{10}. At this voltage, the intrinsic modes in the MF range appear as solitary waves or short bursts (i.e. events that may last from one to several cycles) that are correlated with the decreasing phase of breathing mode cycles. Increasing the voltage to 700 V, one can notice that the intrinsic modes in the MF range turn into irregular but continuous waves with amplitudes comparable to that of the breathing mode – see Fig. 7b. Finally, for $U_d = 900$ V, intrinsic modes within the MF range become more regular (here imf_{10} with average frequency of ≈ 150 kHz) and their amplitude may become even larger than that of the alleged breathing mode (which is possibly represented by imf_{12}) – see Fig. 7c. It is worth noting that the amplitudes of the slowest intrinsic modes that allegedly correspond to the physical breathing mode (with average frequency of the order of 20 kHz) decreases with the growth of U_d. By contrast, the amplitudes of intrinsic modes within the MF range increase with the growth of U_d. Moreover, the instantaneous frequency of these modes tends to stabilize at an average value around 150–200 kHz. This observation has been confirmed in many experimental sessions.

4.2.2. HF range. As mentioned above, the HF emission is usually triggered during the decreasing phase of the I_A cycle and ceases before the discharge current reaches its next maximum. This is obvious for $U_D = 500$ V and is consistent with previous reports for a PPS-100 thruster (Ref. [12, 18]). A similar correlation is observed for $U_D = 900$ V. However, in the latter case the fundamental frequency of the discharge current I_A is much higher (~ 150 kHz) than for $U_D = 500$ V. Moreover, the amplitude of I_A varies irregularly in time. This suggests that the HF emission bursts may be given too little time to rise up to its saturation level in subsequent cycles of I_A. For $U_D = 700$ V, HF emission is very irregular and appears to last permanently, although its onset and fading cannot be reliably estimated.

On the other hand, the bursts of HF emission collected by the P_1, P_2, and P_3 probes exhibit some periods during which oscillations are more regular (wave packets), with average frequencies in the range 50–100 MHz (a sample of imf_{04} extracted from the P_3 probe signal is shown in Fig. 8c). Usually these wave packets last for several cycles and appear in seriess. The time intervals between subsequent packets correspond to an average repetition frequency of about 4–5 MHz. It is worth noting that each series of wave packets is correlated with a deep modulation of the discharge current I_A – e.g. for $U_d = 900$ V, it is correlated with the 150 kHz MF modes. This suggests that, due to fast and deep modulation of I_A, the azimuthal electrostatic wave is not given enough time to develop fully.

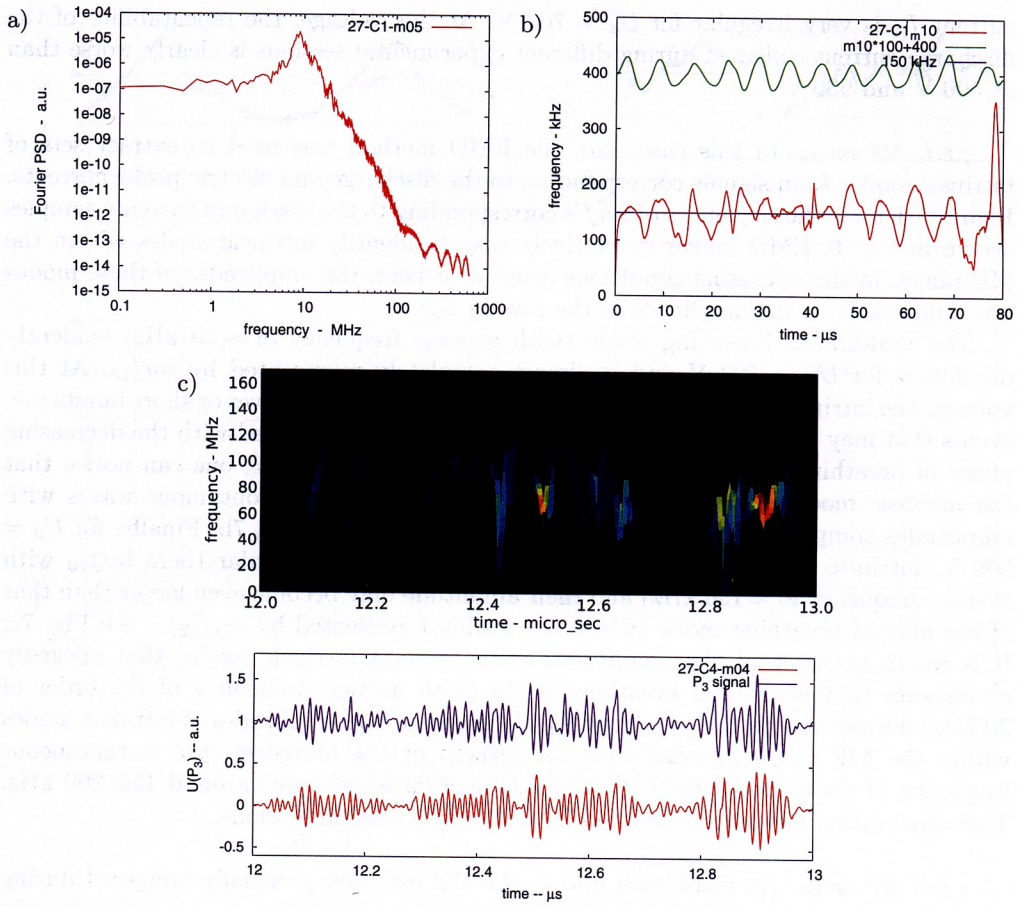

FIG. 8. Spectral characteristics of intrinsic modes samples for $U_d = 900\,\mathrm{V}$ and xenon flow rate 5 mg/s: *a*) Fourier PSD of imf_{05} extracted from I_A with the EMD method, *b*) instantaneous frequency $\nu(t)$ of imf_{10} from the same set of intrinsic modes (red curve) – the rescaled mode imf_{10} is additionally shown in green, *c*) in the upper panel, Hilbert–Huang spectrum of an imf_{04} sample extracted from the P_3 probe signal; in the lower panel, the corresponding sample (in red) and the raw P_3 probe signal (in blue).

5. Conclusion

A new high-voltage HET has been studied over a wide range of operating conditions. The oscillations of global characteristics such as the discharge current and the cathode potential are measured directly in the electrical circuit of the thruster. The local fluctuations of plasma are collected by electric probes located in the exhaust region of the thruster. The empirical mode decomposition method has been used to analyze the recorded non-stationary signals. Characteristic bands of instantaneous frequencies are identified by means of the Hilbert–Huang transform, or for some quasisteady modes, with the use of traditional Fourier methods.

The study of the oscillations of the discharge current and cathode potential for different operating conditions, reveals a number of irregular oscillations superimposed

on the well-known breathing mode. The instantaneous frequency of these oscillations remains in the vicinity of 200 kHz. Their magnitude increases with the discharge voltage, and at 900 V they can become large enough to mask the breathing mode component of the main discharge current. At high discharge voltage, the discharge current oscillations become deep and relatively fast (about 150 kHz), but are more stable than at the lower voltages. By contrast, at lowest discharge voltages or for reduced xenon flow rate, the discharge current I_A appears as a pure breathing mode.

The analysis of the signals collected by electric probes suggests that the regular HF emission previously observed in the PPS-100 thruster occurs only under specific operation conditions in the new thruster. When it occurs, the interpretation of this signal based on electrostatic waves that propagates along the azimuth with the electron drift velocity appears to be reasonably supported. The HF emission is usually broadband (5–200 MHz) and becomes very irregular or even seemingly random at higher discharge voltages. Whether this is the result of a transition to turbulence or of an interference of several azimuthal modes, remains an open question.

It is worth noting that at the highest voltage (900 V), HF emission appears to be correlated with the deep, $\sim$150 kHz modulation of the discharge current. One may legitimately wonder whether this deep modulation of the main discharge current represents transit time oscillations masking the breathing mode, or whether it relates to the breathing mode after its bifurcation from a limit cycle to the invariant torus. We expect the first hypothesis to hold true.

Acknowledgment

This joint work performed by CNRS – France and IPPT-PAN – Poland, was carried out in the frame of the research group "Propulsion par Plasma dans l'Espace" (GDR 3161 CNRS/CNES/SNECMA/Universities).

References

1. O. Duchemin, P. Dumazert, N. Cornu, D. Estublier, and F. Darnon, *Stretching the operational envelope of the PPS®-X000 Plasma Thruster*, Proceedings of the 50th AIAA JPS&E, Joint Propulsion Conference and Exhibit, 11–14 July, 2004, Ft. Lauderdale, FL, AIAA-2004-3605.
2. N.E. Huang, Z. Shen, S.R. Long, M.C. Wu, H.H. Shih, Q. Zheng, N.-C. Yen, C.C. Tung, and H.H. Liu, *The empirical mode decomposition and the Hilbert spectrum for nonlinear and non-stationary time series analysis*, Proc. R. Soc. Lond., **A 454**, 903, 1998.
3. B. Boashash, *Estimating and interpreting the instantaneous frequency of signal: Part I and II*, Proceedings of the IEEE, **80**, 520, 1992.
4. D. Gabor, *Theory of communication*, J. IEE (London), Vol. **93**, Part III, No. 26, (November), 429–457, 1946.
5. L. Cohen, *Time-Frequency Analysis*, Prentice Hall Signal Processing Series, Englewood Cliffs, New Jersey 07632, 1995.
6. T. Yalçinkaya, and Y.-C. Lai, *Phase characterization of chaos*, Phys. Rev. Lett., **79**, 3885, 1997.
7. M. Dätig, and T. Schlurmann, *Performance and limitations of the Hilbert Huang transformation (HHT) with an application to irregular water waves*, Ocean Ingeneering, **31**, 1783, 2004.
8. B. Liu, S. Riemenschneider, and Y. Xu, *Gearbox fault diagnosis using empirical mode decomposition and Hilbert spectrum*, Mechanical Systems and Signal Processing, **20**, 3, 718–734, 2006.

9. J. Kurzyna, S. Mazouffre, L. Albarede, K. Makowski, Z. Peradzyński, M. Dudeck, and G. Bonhomme, *Empirical mode decomposition method in application to analysis of the oscillations in a stationary plasma thruster*, German-Polish Conference on Plasma Diagnostics for Fusion and Applications, Cracow, September 8–10, 2004.

10. L. Albarède, Ph.D. Thesis, University of Orléans, France, 2004.

11. G. Bonhomme, C. Enjolras, J. Kurzyna, S. Mazouffre, L. Albarede, and M. Dudeck, *Characterization of Hall Effect Thruster Plasma Oscillations based on the Hilbert–Huang Transform*, IEPC-2005-46, The 29th International Electric Propulsion Conference, Princeton University, October 31 – November 4, 2005.

12. J. Kurzyna, S. Mazouffre, A. Lazurenko, L. Albarede, G. Bonhomme, K. Makowski, M. Dudeck, and Z. Peradzyński, *Spectral analysis of Hall effect thruster plasma oscillations based on the Empirical Mode Decomposition*, Physics of Plasmas, **12**, 123506, 2005.

13. J. Kurzyna, K. Makowski, A. Lazurenko, S. Mazouffre, M. Dudeck, G. Bonhomme, and Z. Peradzyński, *Search for the frequency content of Hall effect thruster HF electrostatic wave with the Hilbert–Huang method*, PLASMA-2005 International Conference on Research and Applications of Plasmas & 3rd German-Polish Conference on Plasma Diagnostics for Fusion and Applications & 5th French-Polish Seminar on Thermal Plasma in Space and Laboratory, Opole-Turawa, Poland, September 6–9, 2005, pp. 411–414.

14. A. Bouchoule, A. Cadiou, A. Héron, M. Dudeck, and M. Lyszyk, *An overview of the French research program on plasma thrusters for space applications*, Contrib. Plasma Phys., **41**, 573, 2001.

15. A. Lazurenko, L. Albaréde, and A. Bouchoule, *Physical characterization of high-frequency instabilities in Hall thrusters*, Phys. Plasmas, **13**, 083503, 2006.

16. Y. Esipchuck, A. Morozov, G. Tilinin, and A. Trofimov, *Plasma oscillations in closed drift accelerators with an extended acceleration zone*, Sov. Phys. Tech. Phys., **18**, 928, 1974.

17. S. Barral, K. Makowski, Z. Peradzyński, and M. Dudeck, *Transit time instability in Hall thruster*, Phys. Plasmas, **12**, 073504, 2005.

18. A. Lazurenko, V. Vial, M. Prioul, and A. Bouchoule, *Experimental investigation of high-frequency drifting perturbations in Hall thrusters*, Phys. Plasmas, **12**, 013501, 2005.

Received March 27, 2009.